Understanding quantum scattering properties in terms of purely classical dynamics: Two-dimensional open chaotic billiards

J. A. Méndez-Bermúdez,[1] G. A. Luna-Acosta,[1] P. Šeba,[2,3] and K. N. Pichugin[2,4]

[1]*Instituto de Física, Universidad Autónoma de Puebla, Apartado Postal J-48, Puebla 72570, México*
[2]*Department of Physics, University Hradec Kralove, Hradec Kralove, Czech Republic*
[3]*Institute of Physics, Czech Academy of Sciences, Cukrovarnicka 10, Prague, Czech Republic*
[4]*Kirensky Institute of Physics, 660036 Krasnoyarsk, Russia*

We study classical and quantum scattering properties of particles in the ballistic regime in two-dimensional chaotic billiards that are models of electron- or micro-waveguides. To this end we construct the purely classical counterparts of the scattering probability (SP) matrix $|S_{n,m}|^2$ and Husimi distributions specializing to the case of mixed chaotic motion (incomplete horseshoe). Comparison between classical and quantum quantities allows us to discover the purely classical dynamical origin of certain general as well as particular features that appear in the quantum description of the system. On the other hand, at certain values of energy the tunneling of the wave function into classically forbidden regions produces striking differences between the classical and quantum quantities. A potential application of this phenomenon in the field of microlasers is discussed briefly. We also see the manifestation of whispering gallery orbits as a self-similar structure in the transmission part of the classical SP matrix.

I. INTRODUCTION

At present, the majority of studies on the quantum-classical correspondence (QCC) of chaotic systems concern *bounded* motion, for which very important results have been obtained [1–3]. Most works also treat the situation when chaos is *fully* developed. Here we would like to contribute to the understanding of the QCC for *open* systems with *mixed* chaotic motion, in particular, we consider particle motion in two-dimensional (2D) billiards whose phase space is characterized by incomplete (Smale) horseshoes. As is well known, 2D billiards are popular models of ballistic mesoscopic systems [4–6] and microwave cavities [7].

Usually and naturally, QCC is explored by means of semi-classical calculations [8]. Unfortunately, this approach poses limitations since semiclassical quantities involve the cumbersome determination of the action associated with the trajectories and sums which often do not converge. However, as Baranger and co-workers [8] have found through their semi-classical calculations of conductance, the dominant contributions to the average quantum conductance are classical. This motivates us to construct purely classical counterparts of the scattering probability (SP) matrix $|S_{n,m}|^2$ and Husimi distributions for 2D open billiards. In a previous paper [9] we showed that knowledge of the classical counterpart of the SP matrix enables us to predict the global structure of the quantum SP matrix. Here we further our study, specializing to the case of mixed chaotic motion, by: (1) analyzing in more detail the type of trajectories responsible for the formation of certain structures in the classical and quantum SP matrices; (2) comparing Husimi distributions with classical phase space structures; and (3) identifying certain purely quantum effects in the behavior of the conductance.

This paper is organized as follows. In Sec. II we review briefly the general construction of the quantum and classical SP matrices. In Sec. III the 2D waveguide model is presented, as well as its resulting quantum and classical SP ma-

trices for a large number of modes. Section IV concerns the dynamical analysis of the classical SP matrix, the existence of whispering gallery orbits, and the structure that these create in the classical SP matrix. Some aspects of the QCC are studied in Sec. V in terms of the Husimi distribution and its classical counterpart, the *local Poincaré map*. The appearance of purely quantum effects in our system and a possible application is analyzed in Sec. VI. In Sec. VII we make some concluding remarks.

II. QUANTUM AND CLASSICAL SP MATRICES

Quantum scattering is studied via the scattering matrix $\hat{\mathbf{S}}$ which relates incoming to outgoing waves

$$V^{out} = \hat{\mathbf{S}} \, V^{in}, \qquad (1)$$

where the V^{in} and V^{out} vectors specify, respectively, waves coming into and going out of the interaction region. In the case of a 2D waveguide of arbitrary shape connected to two leads of equal width $d_L = d_R = d$, the expression for the energy in the leads is

$$E = \frac{\hbar^2}{2m_e} \left(k_m^2 + \frac{m^2 \pi^2}{d^2} \right), \qquad (2)$$

where k_m and $(m\pi/d)$ are, respectively, the longitudinal and transversal momentum components of the total wave vector $\mathbf{K}$ of magnitude $K = \sqrt{2m_e E}/\hbar$.

The $\hat{\mathbf{S}}$ matrix attains the form (see Ref. [9] for details)

$$\hat{\mathbf{S}} = \begin{pmatrix} t & r' \\ r & t' \end{pmatrix}. \qquad (3)$$

Here, t, t', r, and r' are the transmission and reflection $M \times M$ matrices, where M is the highest mode (the largest transversal mode beyond which the longitudinal wave vector $k_m^{L,R} = \sqrt{(2m_e E/\hbar^2) - (m^2\pi^2/d_{L,R}^2)}$ becomes complex). The elements of the transmission (t and t') and reflection (r and

r') matrices are the transmission and reflection amplitudes given, respectively, by $t_{mn}(E) = (\sqrt{k_n/k_m})a_n^R/a_m^L$, $t'_{mn}(E) = (\sqrt{k_n/k_m})b_n^L/b_m^R$, $r_{mn}(E) = (\sqrt{k_n/k_m})b_n^L/a_m^L$, and $r'_{mn}(E) = (\sqrt{k_n/k_m})a_n^R/b_m^R$. Here, a_m^L (a_n^R) is the amplitude of the forward traveling plane wave $\exp[ik_m^{L,R}(x)]\sqrt{2/d}\sin(m\pi y/d)$ on the left (right) lead corresponding to the mth transversal mode. Similarly, b_n^L (b_m^R) is the amplitude of the backwards traveling plane wave $\exp[-ik_m^{L,R}(x)]\sqrt{2/d}\sin(m\pi y/d)$ on the left (right) lead. See Ref. [9] for details. The *squared* modulo element $|t_{n,m}|^2$($|t'_{n,m}|^2$) gives the probability amplitude for a left (right)-incoming mode m to be transmitted to the right (left) lead into the mode n. Similarly, $|r_{n,m}|^2$ ($|r'_{n,m}|^2$) is the probability for a left (right)-incoming mode m to be reflected to the left (right) lead into mode n.

The SP matrix is defined by the $2M \times 2M$ matrix $|S_{n,m}|^2$, representing the transition probability for the incoming mode m to transmit or reflect into an outgoing mode n.

The connection to the classical description is given by the angle between k_m and K:

$$\theta_m = \sin^{-1}\left[\frac{m\pi}{d}\frac{1}{K}\right] = \sin^{-1}\left[\frac{m\pi\hbar}{d\sqrt{2m_eE}}\right]. \quad (4)$$

Classically, a particle can enter the lead at any angle in the continuous range $-(\pi/2) < \theta < (\pi/2)$, but since the M open modes for a given energy E are discrete, we associate a *range* of angles $\Delta\theta_m \equiv \theta_m - \theta_{m-1}$ to each mode m. That is, we coarse grain the classical angles. Clearly the classical limit is $M = \infty$.

The procedure to construct the purely classical counterpart of $|S_{n,m}|^2$ is the following [9]. Consider a classical particle entering the cavity of the waveguide, say, from the left lead and making an angle θ_i within a range corresponding to a given mode m. The particle (ray) will generally collide with the walls of the cavity of the waveguide a few times before exiting the cavity either to the left or to the right lead, making a certain angle θ_f to which we can associate a mode n if $\theta_f \in \Delta\theta_n$. To specify the initial conditions for the trajectory of the ith particle, the initial position (x_i, y_i) and the initial angle θ_i must be given. In order to account for all possible types of trajectories, we take a large number (typically 10^5) of initial positions for each incoming angle θ_i. By recording the number of particles scattered into the various ranges of θ associated with different outgoing modes n, we obtain a distribution of outgoing modes for each incoming mode m. This distribution gives the *classical counterpart* of the matrix elements $|t_{n,m}|^2$ and $|r_{n,m}|^2$ of the quantum SP matrix. Similarly, to obtain the classical counterpart of $|t'_{n,m}|^2$ and $|r'_{n,m}|^2$ we repeat the above process, but for particles entering from the right lead. This defines the procedure for constructing the *classical* SP *matrix*.

III. THE SYSTEM

We chose the geometry of the cavity of the waveguide to be that of a rippled billiard, which consists of two hard walls: a rippled wall modulated by a periodic function $y(x) = d + a\xi(x)$ [$\xi(x+L) = \xi(x)$], and a flat wall at $y = 0$; d is
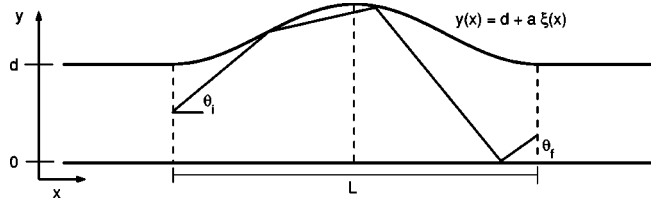

FIG. 1. Geometry of the waveguide. $\xi(x) = 1 - \cos(2\pi x/L)$. The three fundamental orbits of the cavity are shown in dashed lines.

the width of the waveguide and a is the amplitude of the ripple. For concreteness, the periodic function in this paper is given by $\xi(x) = 1 - \cos(2\pi x/L)$, which defines the *cosine billiard* also analyzed extensively by Ketzmerick and co-workers [5,10]. Our waveguide system is defined by a cavity formed by a *single* period of the cosine billiard attached to two aligned semi-infinite leads each of width d, see Fig. 1.

This *finite* length version of the rippled billiard, a model of a quantum or electromagnetic waveguide, has been used to study certain transport manifestations of chaos in the classical [11,12] and quantum [5,6,9,10] regimes. Moreover, studies of the *infinitely* long (periodic with no leads) rippled billiard, originally introduced to model beam acceleration problems [13], has also provided insight in the understanding of general features of periodic structures (e.g., energy band structure, structure of eigenfunctions, etc.) and has been utilized to explore the problem of quantum-classical correspondence of classically chaotic systems [14–16].

The most useful tool to obtain the whole panorama of the classical dynamics of a bounded system (e.g., a closed or periodic billiard) is the phase portrait given by the Poincaré map (PM) of a representative set of initial conditions (see, e.g., Ref. [11]). However, for an unbounded system such as our waveguide, its Smale horseshoe is more appropriate since it gives the topology of the homoclinic tangle which completely characterizes the scattering dynamics, connecting the interacting region with the asymptotic regions [17]. For our waveguide, the domain of the interacting region is the cavity, while the asymptotic regions are the leads. The number of fundamental orbits (period-one periodic orbits) determine the order of the horseshoe. Our cavity (for $a > 0$) has three of them (shown in dashed lines in Fig. 1) and hence its horseshoe is ternary [18]. In Fig. 2 we present the horseshoe of the system (stable and unstable manifolds) where only the tendrils up to the hierarchy level three are plotted using the parameters $(d, a, L) = (1.0, 0.305, 5.55)$. In particular, for this set of parameters the horseshoe is incomplete with a ''development parameter'' γ slightly less than 3^{-2}, a typical situation of mixed phase space [19].

For the set of parameters used, we obtain a period-one and a period-four resonance islands, see also Fig. 2. These islands are formed by trapped orbits bouncing in the neighborhood of stable periodic orbits. In particular, the central resonance is formed by trajectories colliding nearly perpendicular with the walls in the neighborhood of $x = L/2$, the widest part of the cavity, see Fig. 1. Note that the orbits within these islands are *classically not* accessible to scattering trajectories.

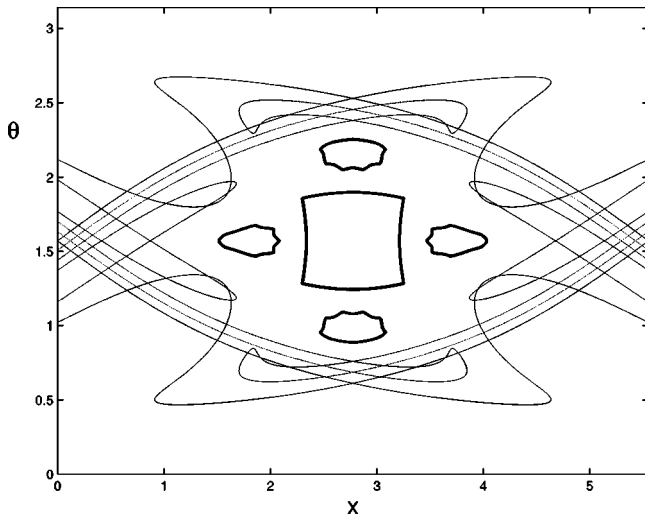In Figs. 3 and 4 we present, respectively, the quantum and

FIG. 2. Ternary horseshoe of the system ($\gamma \lesssim 3^{-2}$) using as surface of section the bottom boundary of the cavity for $(d,a,L) = (1.0, 0.305, 5.55)$. The tendrils up to level three are plotted. The KAM curves (thick lines) around the period-one and period-four resonance islands are superimposed in the plot.

classical SP matrix for the *one-period* waveguide with $M = 200$ open channels. The quantum SP matrix was calculated by the recursive Green's function method [5,10], and the classical SP matrix by the procedure described above with 10^3 ensembles (each characterized by a different θ_i) of 10^5 different initial conditions. Note the rich structure present mainly in the transmission part ($|t_{n,m}|^2$ and $|t'_{n,m}|^2$) of the SP matrix. We note that $t = t'$ and $r = r'$, as expected from the symmetry of the system.

The similarity between quantum and classical SP matrices is remarkable in the case of a large number of modes (here $M = 200$), suggesting that the motion belongs to the deep
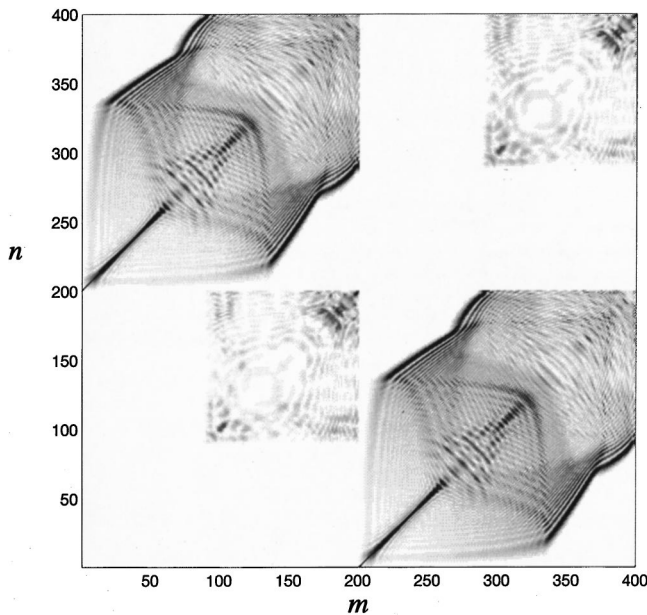

FIG. 3. Quantum SP matrix $|S_{n,m}|^2$ for the one-period waveguide with $(d,a,L) = (1.0, 0.305, 5.55)$, and $M = 200$.
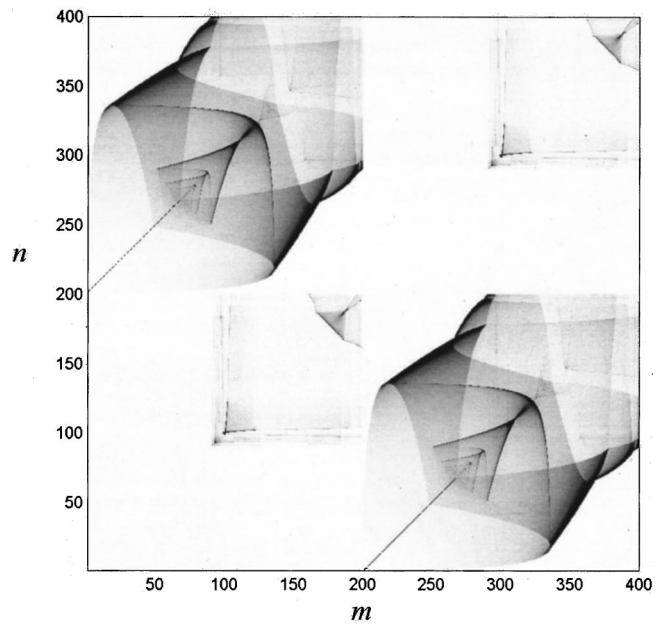

FIG. 4. Classical SP matrix $|S_{n,m}|^2$ for the one-period waveguide with $(d,a,L) = (1.0, 0.305, 5.55)$, and $M = 200$.

semiclassical regime. Nevertheless, we have also seen a resemblance between the quantum and classical SP matrices even for a number of modes as low as ten. Hence the calculation of the classical SP matrix as a tool for prediction becomes relevant in the quantum regime.

IV. DYNAMICAL ANALYSIS OF THE CLASSICAL SP MATRIX

First we focus on the transmission part of the classical SP matrix which is presented in Fig. 5, this time as a function of
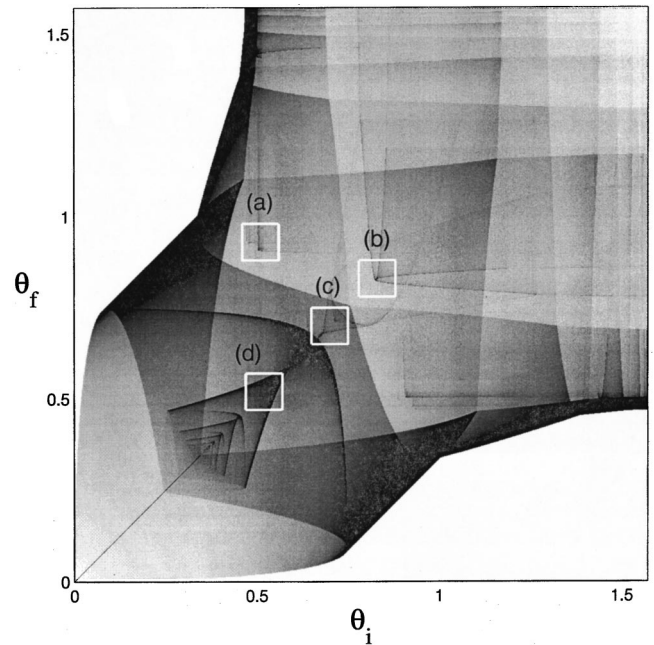

FIG. 5. Transmission part $|t_{n,m}|^2$ of the classical SP matrix as a function of angles.
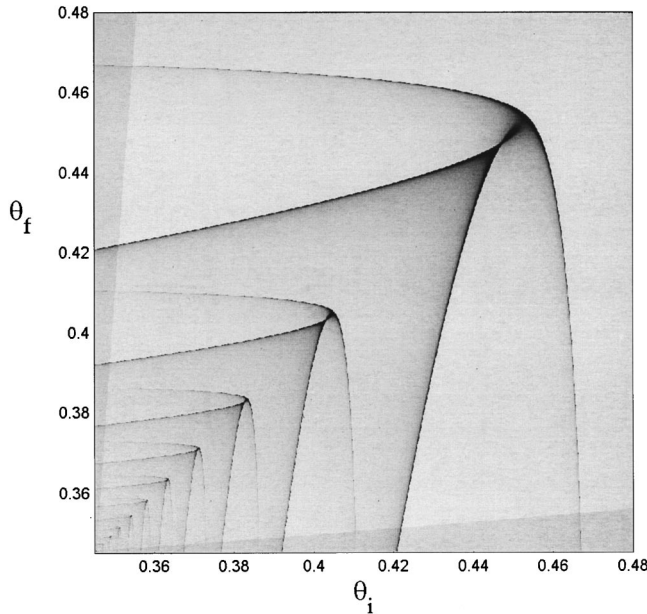
FIG. 6. Enlargement of the transmission part of the classical SP matrix for $0.345 \leq \theta \leq 0.48$.

angles. An interesting structure to analyze is in the region $0.345 \leq \theta \leq 0.48$, for which an enlargement is shown in Fig. 6. The existence of *whispering gallery orbits* (WGO) is well known in cavities with concave walls (note that our cavity has a concave part in $L/4 < x < 3L/4$). These are guided orbits along the inner surface of such cavities, see e.g., Ref. [20]. In recent works, it has been shown that WGOs produce fractal structures in, e.g., "virtual images" of billiards [21]. Here we can see that a self-similar structure, perhaps nonfractal, also shows up in the SP matrix, in particular, in the transmission part of the classical SP matrix (Fig. 6).

We find that the structure of Fig. 6 is formed by trajectories that hit only on the concave part of the *upper* boundary before being transmitted: the outer part of the structure ($\theta > 0.465$) is due to trajectories that hit it only once; the second generation ($\theta \simeq [0.41, 0.465]$) is due to trajectories that hit it twice, the next generation ($\theta \simeq [0.39, 0.41]$) is due to trajectories that hit the boundary three times, and so on, see
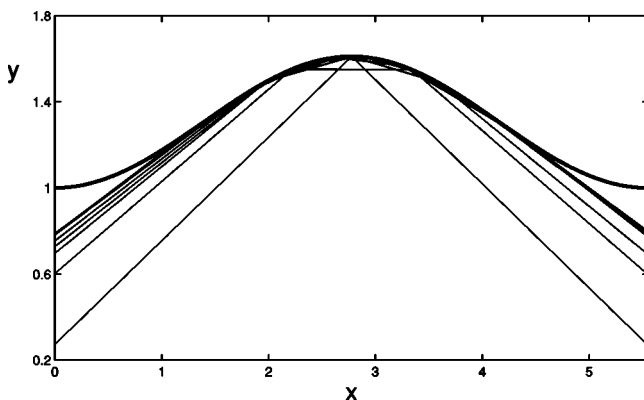

FIG. 7. Trajectories that contribute to the first six generations of the structure of Fig. 6 are shown.
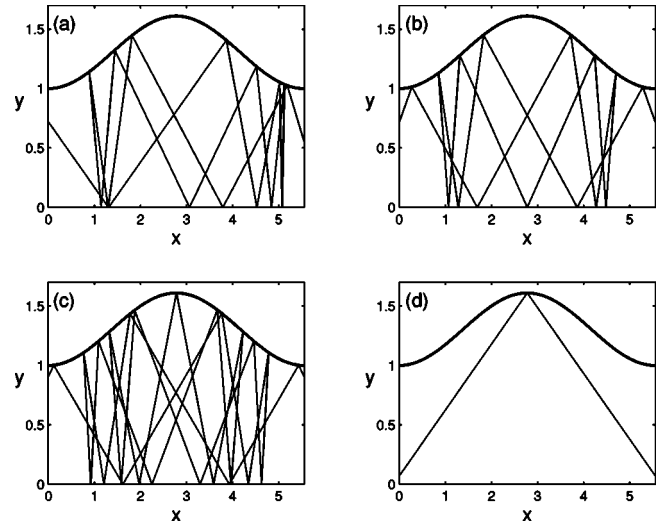

FIG. 8. Typical trajectories that contribute to the zones marked in Fig. 5.

Fig. 7 (a similar result has been reported in Ref. [22] for a different type of billiard). The point of convergence of the self-similar structure (not shown in Fig. 6) can be easily calculated: $\theta = 0.3325$, the angle at the inflection point of the profile ($x = L/4$). A particle that would hit the upper boundary at $x = L/4$ with $\theta_i = 0.3325$ would hit the concave part of the billiard an infinite number of times before leaving it at an angle $\theta_f = 0.3325$.

Similarly, we can discover the types of particle motion that produce the various structures in the transmission part of the classical SP matrix. Fig. 8 shows typical trajectories that contribute to the zones marked in Fig. 5. All these orbits are very stable, small variations of the initial conditions (x_i, y_i, θ_i) follow closely the same trajectory, with the same number of collisions with the upper and lower boundaries and with very similar final angles θ_f. Noting that the matrix elements $|S_{n,m}|^2$ give a measure of the number of trajectories connecting a pair of angles $\theta_i \rightarrow \theta_f$, then for *every high intensity structure in the classical* SP *matrix there corresponds a boundle of stable trajectories*. Moreover, since all the high intensity structures present in the classical SP matrix are also present in its quantum counterpart we can expect the stable orbits of the underlying classical motion to play the dominant role in determining quantum transport properties.

V. LOCAL POINCARÉ MAP

To further analyze our waveguide system we shall use the *local Poincaré map* which has the same meaning as the PM, but now constructed only from the images of incoming trajectories in the cavity region. Since these eventually leave the cavity region, they are transient. The local PM (with surface of section at $y = 0$) is presented in Fig. 9; Fig. 9(a) shows the part of the local PM generated by trajectories whose initial conditions start in the left lead only and Fig. 9(b) shows the contribution of trajectories starting from both, right and left leads. Comparison of Figs. 9(b) and (2) shows, as expected, that the resonance islands produced by bounded motion inside the cavity (see Fig. 2) are forbidden phase
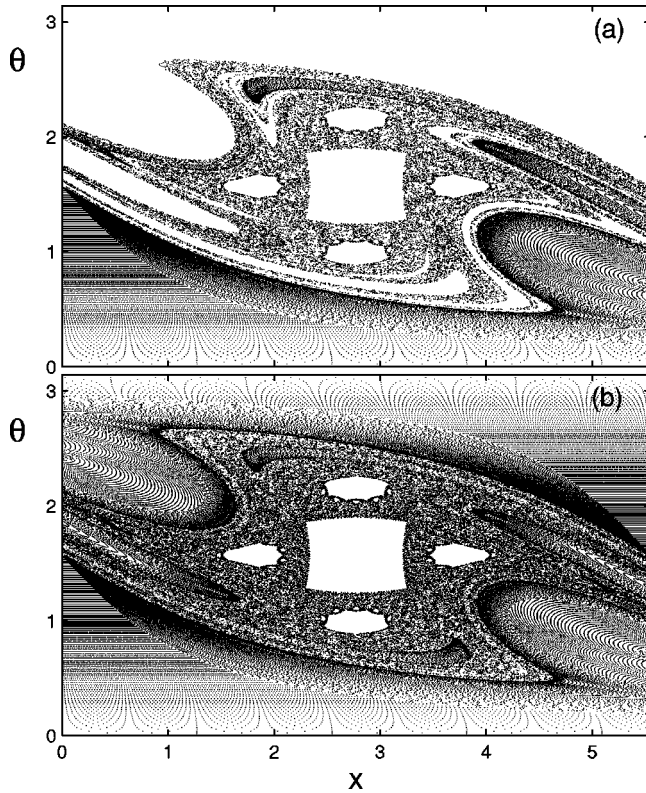
FIG. 9. Local Poincaré map generated by particles entering to the cavity of the waveguide (a) from the left lead and (b) from both leads. In both cases the Poincaré surface of section is located at $y = 0$.
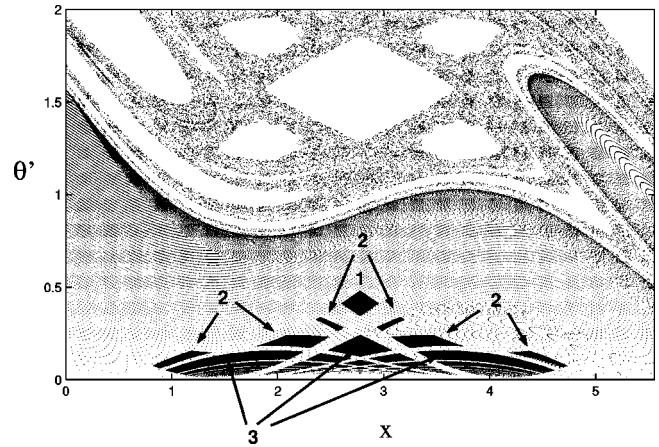

FIG. 10. Local Poincaré map with Poincaré surface of section at the top boundary and the location (highlighted) of the WGOs that contribute to the structure of Fig. 6.

space regions in the local PM. Also note that the structure of the local PM shadows the unstable manifold of the ternary horseshoe of the system, clearly visible up to the tendril of level three. The stable manifold is not present in the structure of the local PM because for the construction of the horseshoe, time-reversed trajectories are included, which is not the case for the local PM.

Now we can ask about the location in the local PM of the WGO. For this purpose we construct the local PM choosing now as surface of section the *top* boundary because, as explained in Sec. IV, the WGOs are guided orbits along the concave part of the boundary. The upper local PM is constructed by the pairs (x_j, θ'_j) corresponding, respectively, to the longitudinal component of the position and the angle made by the total momentum with the tangent of the boundary at x_j, right after the jth collision with the upper wall. The location of the WGO in the local PM is shown (highlighted) in Fig. 10, where the numbers label the number of collisions the particles make with the upper boundary. A structure of this type in phase space formed by WGOs has been reported in Ref. [22]. We see that this pattern evolves from top to bottom; the higher the number of collisions with the upper wall, the closer the angle θ' is to zero. In the limit $\theta' = 0$, a particle will collide an infinite number of times along the concave part of the boundary.

A popular tool used to explore quantum-classical correspondence in billiards is the Husimi distribution [23]; it is the projection of a given quantum state onto a coherent state

of minimum uncertainty. The Husimi distribution can be viewed as a quantum phase space probability density that can be directly compared with the classical phase space. See Ref. [14] for details of the calculation of the Husimi distributions for the infinitely periodic rippled billiard. In a recent work [10], the Husimi distributions were used in the cosine billiard to show, among other things, the relation between the scattering resonances and the eigenstates of the corresponding closed system. Here, for our waveguide system we calculate the Husimi distributions for each one of the m opened modes at certain Fermi energy and compare them with the local PM generated solely by trajectories starting with the corresponding $\Delta\theta_m$ (note that the Husimi distributions for the scattering states reported in Ref. [10] are superpositions of several modes). Then, using a Fermi energy that supports 20 modes, we present in Figs. 11(a)–11(d) the local PM generated by particles entering from the left lead with angles corresponding to the 2nd, 5th, 10th, and 20th mode, respectively, to-
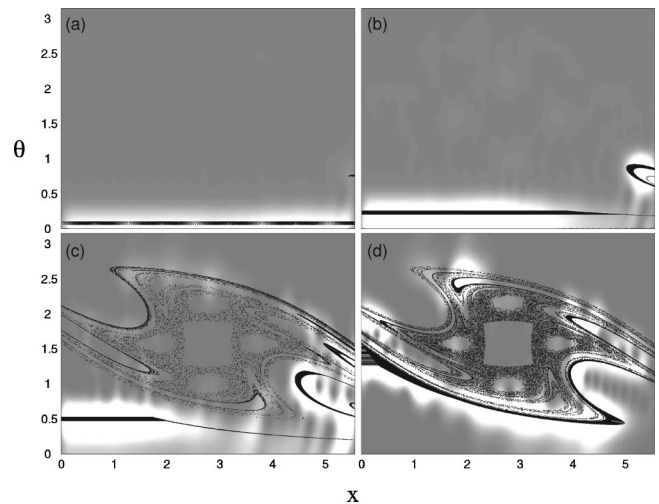

FIG. 11. Local Poincaré maps for the modes (a) 2nd, (b) 5th, (c) 10th, and (d) 20th for particles from the left lead (black dots) and the corresponding Husimi distribution (grayish). The Poincaré surface of section is $y = 0$.
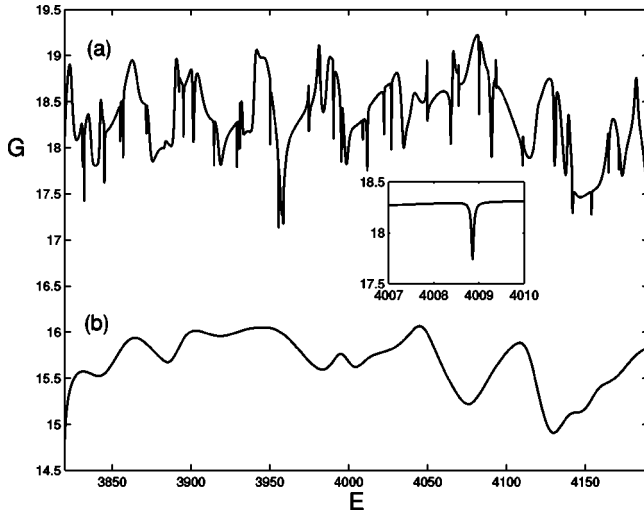
FIG. 12. Dimensionless conductance G for the range of energy that supports 20 modes for the (a) mixed case, $(d,a,L)=(1, 0.305, 5.55)$; and (b) chaotic case, $(d,a,L)=(1, 0.305, 2.77)$. $E=E/E^*$ $\sim M^2\pi^2$, where $E^*=(\hbar^2/2m_e)1/d^2$.
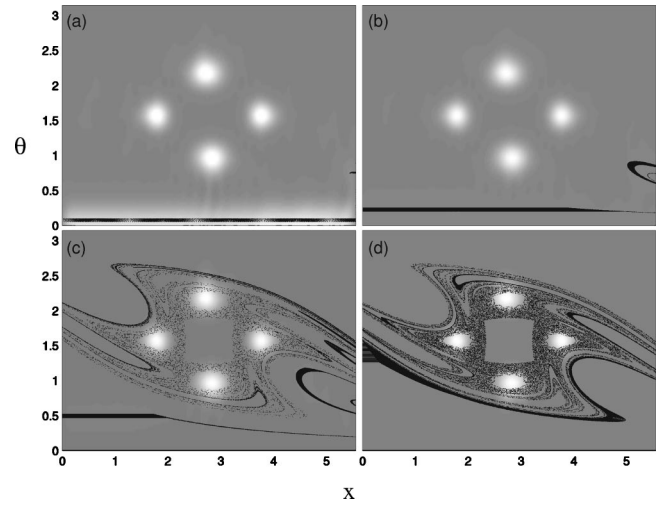

FIG. 13. Local Poincaré maps for the modes (a) 2nd, (b) 5th, (c) 10th, and (d) 20th for particles from the left lead (black dots) and the corresponding Husimi distribution (grayish). The Poincaré surface of section is $y=0$. The resonant energy of the inset of Fig. 12 is used.

gether with the corresponding Husimi distributions. Note that Husimi distributions coincide with the regions of phase space with the largest density of points. This agreement suggests that the local PM can be used to predict, at last qualitatively, the Husimi distributions.

VI. PURELY QUANTUM FEATURES

Recently, Ketzmerick and co-workers [5,10] obtained important results concerning the transport properties of waveguides which classically produce fully chaotic or mixed dynamics. They showed that the behavior of the Landauer conductance G (given by $(2e/\hbar^2)\Sigma_n\Sigma_m|t_{n,m}|^2$, where $t_{n,m}$ are the transmission elements of the S matrix) and the Wigner delay time can clearly distinguish between full and mixed chaos. See also Ref. [6]. In our geometry, this distinction is exemplified in Fig. 12, where we contrast the dimensionless conductance G, in a range of energy that supports 20 modes, for the cases of mixed [Fig. 12(a)] and globally chaotic dynamics [Fig. 12(b)]. For the mixed case we used the same geometrical parameters as before $[(d,a,L)$ $=(1.0,0.305,5.55)]$ and for the globally chaotic case we use $(d,a,L)=(1.0, 0.305, 2.77)$. The difference is clear: while for mixed dynamics the conductance G fluctuates strongly with sharp resonances, for global chaos it is a smooth function of energy. These wild fluctuations in the mixed chaos case are due to the existence of resonances and hierarchical states, as argued in Refs. [5,10].

So far we have seen that the similarity between the classical SP matrix and its quantum counterpart enabled us to understand various quantum features in terms of purely classical dynamics (see also Ref. [9]). We have also seen a nice agreement between the local PM and its quantum counterpart, the Husimi distributions. The energies for which such a good agreement occurs were chosen at random. However, if we select now an energy value corresponding to a sharp dip or peak (isolated resonances) in the conductance (mixed

case), we find substancial differences between the classical and quantum quantities. As an example, in Fig. 13 we plot the same modes as in Fig. 11, but with an energy corresponding to a typical dip in the conductance, see inset of Fig. 12. Note that in contrast with Fig. 11 the Husimis *lie predominantly within the four-period resonance islands* of phase space. The interior of these islands are clearly unaccesible to *classical* particles coming into or going out of the cavity. In contrast, as Fig. 13 indicates, a *quantum* particle can be found within these classical unaccesible regions. The culprit of this phenomenon is Heisenberg's uncertainty principle that allows the wave function to tunnel through the KAM (Kolmogorov-Arnold-Moser) barriers. Since the one-period and four-period islands in phase space are formed by motion within the cavity, they must (and do) appear for the corresponding closed cosine billiard (hard walls at $y=0$, L instead of leads). Hence it is expected that to each scattering state, which produces an isolated resonance in the conductance, there corresponds an energy eigenstate of the closed billiard. In fact, very recently Bäcker, *et al.* [10] used the same cosine billiard model to demonstrate that this is indeed the case, where the scattering states, belonging to the *sharpest* conductance resonances can be identified by energy and Husimi distributions with energy eigenstates living in the resonance islands, and the less sharp conductance resonances with eigenstates whose support is in the hierarchical regions of phase space.

It is also instructive to look at the wave functions in configuration space for the nonresonant and resonant cases, see Fig. 14. The plots on the left (right) of this figure correspond to the nonresonant (resonant) case. The nonresonant (resonant) energy is the same as that used in Fig. 11 (Fig. 13) for modes 2, 5, and 20. These plots reveal a striking difference. In the resonant case we notice a *M*-shaped pattern that shadows the classical trajectory of a particle in a four-period periodic orbit, corresponding to the four islands in the local PM. As mentioned above, the phase space region of the pe-
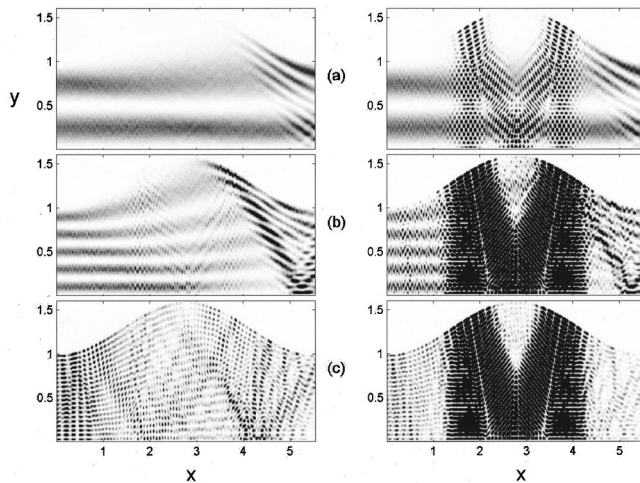
FIG. 14. Wave functions for the modes (a) 2nd, (b) 5th, and 20th for a nonresonant (left column) and the resonant energy of the inset of Fig. 12 (right column).

riod four islands is not accessible to *classical* particles incoming from the right or left leads; only trajectories originated in the interior of the cavity can be trapped and form this pattern. It is precisely this M-shaped pattern that has been exploited experimentally in Ref. [24] for the construction of high gain microlasers with directional emission with *closed* resonators of high refractive index. We see that such a pattern can be obtained also for *open* cavities because quantum mechanically the wave function, due to Heisenberg's uncertainty, can penetrate into the classically forbidden areas. Thus, as we have proposed in Ref. [25], directional emission microlasers may also be constructed with open cavities. We have also computed ''classical wave functions'' for these type of cavities, constructed basically in the same way as the local PM with a box-counting method to mimic intensity in configuration space [26]. The classical wave functions that we obtained look very much like the truly quantum wave functions for the nonresonant case except for interference patterns. Of course, the classical wave functions do not reproduce the resonance structure as this is a purely quantum effect.

VII. CONCLUDING REMARKS

The objective of this work has been to contribute to the understanding of the classical-quantum correspondence as regards scattering in open billiards which serve as models of mesoscopic electron waveguides as well as microwave cavities. Here we make a comparative analysis between the scattering probability (SP) matrix and the Husimi distributions

with their classical counterparts, namely, the classical SP matrix and the local Poincaré maps, respectively. As a paradigm of open billiards, we use a model of a ballistic 2D waveguide formed by a rippled cavity attached to two collinear leads. The classical particle motion in such cavity is known to undergo the generic Hamiltonian transition to chaos [5,6,11–16]. For the purpose of this work, the parameters of the cavity were chosen to produce a ternary incomplete horshoe (mixed chaos).

We find a very good global similarity between classical and quantum SP matrices and, as expected, this similarity is greater as the number of open modes in the quantum system increases. However, even for a moderate number of modes (~ 10–20) the similarity between classical and quantum SP matrices allows us to extract important information about general as well as individual features of the quantum system. In particular, all high intensity patterns in the classical SP matrix, found to be produced by bundles of stable trajectories, appear also in the quantum SP matrix. Hence, from the knowledge of the structure of the *classical* SP matrix we can predict which incoming modes contribute dominantly to transmission or reflection in the quantum system [9]. We have also shown that certain self-similar structure in the transmission part of the classical SP matrix is due to whispering gallery orbits (WGO).

On the other hand, important differences occur for energy values corresponding to sharp peaks or dips in the conductance. For these resonant energies, the wave functions tunnel (thanks to Heisenberg's uncertainty principle) into forbidden classical phase space regions (resonance islands), associated with stable periodic orbits within the cavity.

Similarly, the Husimi distributions and the local PM show an excellent agreement in the case of nonresonant energies. The agreement suggests the usefulness of the local PM as a tool to predict the support of Husimi distributions for each open mode in the system. Also, we have seen that for a certain resonant energy, where substantial differences between local PM and Husimi distributions occur, the wave functions of the system form a M-shaped pattern. We have exploited this phenomenon to propose the construction of microlaser resonators in open cavities [25].

[1] F. M. Izrailev, Phys. Rep. **196**, 299 (1990); and F. Haake, *Quantum Signatures of Chaos* (Springer, Berlin, 1991).

[2] M. C. Gutzwiller, *Chaos in Classical and Quantum Mechanics* (Springer-Verlag, New York, 1990); L. E. Reichl, *The Transition to Chaos in Conservative Classical Systems: Quantum Manifestations* (Springer-Verlag, New York, 1992).

[3] H-J. Stockmann, *Quantum Chaos: an Introduction* (Cambridge University Press, Cambridge, UK, 1999).

[4] See for example, J. Imry, *Introduction to Mesoscopic Systems* (Oxford University Press, New York, 1997); and S. Datta,

Electron Transport in Mesoscopic Systems (Cambridge University Press, Cambridge, 1995).

[5] B. Huckestein, R. Ketzmerick, and C. H. Lewenkopf, Phys. Rev. Lett. **84**, 5504 (2000).

[6] Gursoy B. Akguc and L. E. Reichl, J. Stat. Phys. **98**, 813 (2000).

[7] See for example, Chap. 2 in Ref. [3] and C. Dembowski, H.-D. Gräf, R. Hofferbert, H. Rehfeld, A. Richter, and T. Weiland, Phys. Rev. E **60**, 3942 (1999).

[8] H. U. Baranger, R. A. Jalabert, and A. D. Stone, Phys. Rev. Lett. **70**, 3876 (1993); H. U. Baranger, R. A. Jalabert, and A. D. Stone, Chaos **3**, 665 (1993); H. U. Baranger, D. P. Vincenzo, R. A. Jalabert, and A. D. Stone, Phys. Rev. B **44**, 10 637 (1991); and H. U. Baranger, Physica D **83**, 30 (1995).

[9] G. A. Luna-Acosta, J. A. Méndez-Bermúdez, P. Šeba, and K. N. Pichugin, Phys. Rev. E **65**, 046605 (2002).

[10] A. Bäcker, A. Manze, B. Huckestein, and R. Ketzmerick, e-print arXiv:nlin.CD/0201057 (2002).

[11] A. J. Lichtenberg and M. A. Lieberman, *Regular and Chaotic Dynamics*, 2nd ed. (Springer-Verlag, New York, 1992), Sec. 6.1(b).

[12] G. A. Luna-Acosta, A. A. Krokhin, M. A. Rodriguez, and P. H. Hernandez-Tejeda, Phys. Rev. B **54**, 11 410 (1996).

[13] J. L. Tennyson, in *Nonlinear Dynamics and the Beam-Beam Interaction*, edited by M. Month and J. C. Herrera, AIP Conf. Proc. No. **57** (AIP, New York, 1979), p. 158.

[14] G. A. Luna-Acosta, K. Na, L. E. Reichl, and A. Krokhin, Phys. Rev. E **53**, 3271 (1996).

[15] G. A. Luna-Acosta, J. A. Méndez-Bermúdez, and F. M. Izrailev, Phys. Lett. A **274**, 192 (2000).

[16] G. A. Luna-Acosta, J. A. Méndez-Bermúdez, and F. M. Izrailev, Phys. Rev. E **64**, 036206 (2001).

[17] S. Smale, Bull. Am. Math. Soc. **73**, 747 (1967).

[18] See. e.g., W. Breymann and C. Jung, Europhys. Lett. **25**, 509 (1994); C. Lipp and C. Jung, J. Phys. A **28**, 6887 (1995).

[19] B. Rückerl and C. Jung, J. Phys. A **27**, 55 (1994).

[20] J. U. Nöckel and A. D. Stone, Nature (London) **385**, 45 (1997).

[21] C. A. Kruelle, A. Kittel, J. Peinke, and R. Richter, Z. Naturforsch., A: Phys. Sci. **52**, 581 (1997).

[22] R. G. Nazmitinov, K. N. Pichugin, I. Rotter, and P. Šeba, Phys. Rev. E **64**, 056214 (2001).

[23] K. Husimi, Proc. Phys. Math Soc. Jpn. **22**, 246 (1940); B. Crespi, G. Perez, and S.-J. Chang, Phys. Rev. E **47**, 986 (1993).

[24] C. Gmachl, F. Capasso, E. E. Narimanov, J. U. Nöckel, A. D. Stone, J. Faist, D. L. Sivco, and A. Y. Cho, Science **280**, 1556 (1998).

[25] J. A. Méndez-Bermúdez, G. A. Luna-Acosta, and P. Šeba, Phys. Status Solidi B **230**, 385 (2002).

[26] J. A. Méndez-Bermúdez and G. A. Luna-Acosta (unpublished).